PCCP

PAPER

View Article Online
View Journal | View Issue



Cite this: *Phys. Chem. Chem. Phys.*, 2024, **26**, 11360

# Phosphonic acid anchored tripodal molecular films on indium tin oxide†

Chaoran Zhang,[a] Saunak Das,[a] Naoya Sakurai,[b] Takaki Imaizumi,[b] Sajisha Sanjayan,[b] Yoshiaki Shoji,[b] Takanori Fukushima *[bc] and Michael Zharnikov *[a]

Received 29th February 2024,
Accepted 27th March 2024

DOI: 10.1039/d4cp00892h

rsc.li/pccp

Whereas monopodal self-assembling monolayers (SAMs) are most frequently used for surface and interface engineering, tripodal SAMs are less popular due to the difficulty in achieving a reliable and homogeneous bonding configuration. In this context, in the present study, the potential of phosphonic acid (PA) decorated triptycene (TripPA) for formation of SAMs on oxide substrates was studied, using indium tin oxide (ITO) as a representative and application-relevant test support. A combination of several complementary experimental techniques was applied and a suitable monopodal reference system, benzylphosphonic acid (PPA), was used. The resulting data consistently show that TripPA forms well-defined, densely packed, and nearly contamination-free tripodal SAMs on ITO, with the similar parameters and properties as the monopodal reference system. Modification of wetting properties and work function of ITO by non-substituted and cyano-decorated TripPA SAMs was demonstrated, showing a potential of this tripodal system for surface engineering of oxide substrates.



## 1. Introduction

Controlled engineering of surfaces and interfaces is one of the key issues of modern nanotechnology. An important approach in this context is molecular self-assembly. The respective nanometer-thin molecular films, termed self-assembled monolayers (SAMs), can modify significantly physical and chemical properties of surfaces and interfaces and form a template for further chemical reactions, including specific recognition of targeted species.[1–4] These films can also serve as a basis for nanofabrication[5,6] and perform specific electronic functions in different devices.[7–11] The SAM-forming molecules have usually a rod-like character and consist of anchoring group, backbone, and functional tail group.[1,2] The anchoring group is responsible for bonding to the substrate, which varies from weak to strong chemisorption. The tail group constitutes the SAM–ambient interface defining its chemical character and affecting its physical properties. The backbone links the anchoring and tail groups, driving the self-assembly during the SAM formation and contributing to the film stability afterwards.

In most cases, monopodal anchoring groups are used.[1] However, multipodal anchoring is frequently used as well, with the advantages of better electronic coupling to the substrate, higher thermal stability, and additional control of the tail group density.[12–14] Among different multipodal configurations, tripodal-anchored molecules are probably most popular,[15–25] since all three anchoring groups can be potentially placed within the plane of the SAM–substrate interface, corresponding to the desired adsorption mode. However, regretfully, reliable tripodal anchoring is rarely achieved by molecular tripods, which mostly feature inhomogeneous bonding configurations, with some of the anchoring groups decoupled from the substrate, weakly coupled to it, or bonded to each other.

A promising system in this context is a family of triptycene-based molecules, applied successfully on a variety of substrates.[26–33] The triptycene scaffold consists of three phenyl rings coupled together by an aliphatic linker. It can be flexibly functionalized with suitable anchoring groups at the *para*-positions of the rings, providing then a good prerequisite for tripodal anchoring. Complementary, it can be attributed with a variety of functional tail groups at either the opposite *para*-positions of the rings or at the bridgehead position of the linker. So far, nitrile, ethynyl, and ferrocene tail groups were tried in the context of charge transfer phenomena, on-surface click reaction, and molecular electronics.[29,31,33] As to the anchoring groups, thiol, suitable for coinage metals,[26,29,31–33] and carboxylic acid, suitable for Ag[28] and oxide substrates[30] were successfully tested.

[a] *Angewandte Physikalische Chemie, Universität Heidelberg, Im Neuenheimer Feld 253, D-69120 Heidelberg, Germany. E-mail: Michael.Zharnikov@urz.uni-heidelberg.de*
[b] *Laboratory for Chemistry and Life Science, Institute of Innovative Research, Tokyo Institute of Technology, 4259 Nagatsuta, Midori-ku, Yokohama 226-8503, Japan. E-mail: fukushima@res.titech.ac.jp*
[c] *Living Systems Materialogy (LiSM) Research Group, International Research Frontiers Initiative (IRFI), Tokyo Institute of Technology, 4259 Nagatsuta, Midori-ku, Yokohama 226-8501, Japan*

† Electronic supplementary information (ESI) available. See DOI: https://doi.org/10.1039/d4cp00892h

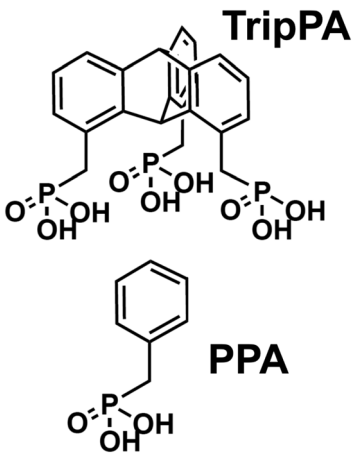


Fig. 1 Molecular structure of the target tripodal system, TripPA, along with the reference monopodal system, PPA. The drawings correspond to the ideal, 'upright' orientation of the molecules in the SAMs.

The most popular anchoring group for oxide substrates is, however, not carboxylic but phosphonic acid (PA), in view of the robust anchoring chemistry and enhanced thermal and chemical stability.[34] Therefore, PA SAMs are frequently used for interfacial engineering of oxide substrates,[34–40] above all in the context of organic electronics and photovoltaics.[34,35,39,41,42] To this end, in the present study, we tested the monomolecular assembly of PA-decorated triptycene (TripPA, Fig. 1) on a model oxide substrate – indium tin oxide (ITO). This transparent and conductive support is not only a suitable test system but is of importance on its own, in view of its broad applications as an electrode material in organic transistors, organic light emitting devices, and organic and perovskite solar cells.[34,35,39,41,42] As a direct reference to the tripodal TripPA molecule, we used monopodal benzylphosphonic acid (PPA, Fig. 1), corresponding to the individual 'blade' of TripPA.

# 2. Experimental

## 2.1. Materials and methods

The synthesis and purification procedure for TripPA is described in the ESI,† which also contains the respective characterization data. The synthesis of NC-Trip-PA, tested by us in the context of work function engineering (see below), was performed within a newly developed multistep procedure, with characterization of synthetic intermediates at each stage. The detailed synthetic procedure will be reported elsewhere. The full characterization data for NC-Trip-PA are presented in the ESI.† PPA was purchased from Sigma-Aldrich and used as received. All other chemicals and solvents were also purchased from Sigma-Aldrich.

As the substrates, ITO-coated glass slides, purchased from Sigma-Aldrich (703192), were used. According to the specification, the ITO films had a surface resistivity of 8–12 $\Omega\ sq^{-1}$. The substrates were cleaned following a literature protocol.[30,43,44] As the first step, they were sequentially cleaned by copious amounts of hot water ($\sim$70 °C), chloroform, and isopropanol. Afterwards, the substrates were immersed in cold isopropanol and kept there for 24 h. Finally, they were exposed to ultraviolet light (254 nm) for 30 min under ambient conditions, and immediately used for the SAM fabrication.

The root-mean-square (RMS) roughness value of the resulting substrates was estimated at $\sim$1.7 nm. It was measured by atomic force microscopy in tapping mode over a 5 μm × 5 μm scan area.[30] Note that the effect of the SAMs on the surface roughness was not specifically monitored since no noticeable changes were expected, based on our preliminary experience.[45,46]

## 2.2. SAM fabrication

The freshly cleaned (blank) ITO substrates were immersed in the solution of TripPA (0.1 mM) in ethanol for 48 h. After the immersion, the samples were carefully dried with soft blow of $N_2$ or Ar. Afterwards, the samples were annealed at 200 °C for 2 h which is the standard fabrication step for PA SAMs (see, *e.g.*, ref. 45 and 46) allowing to promote the robust bonding to the substrate.[34] Finally, the samples were washed repeatedly with ethanol to remove residual physisorbed material and dried with $N_2$ or Ar.

The PPA monolayers were prepared in the same fashion, using the same precursor concentration and the same solvent. The cyano-substituted TripPA SAM was prepared from dimethyl sulfoxide (DMSO); the concentration of the precursor was 0.1 mM. The choice of DMSO instead of ethanol was related to the low solubility of this substance in the latter solvent and to the prevention of possible acidification of the terminal –CN groups.

## 2.3. Characterization

The target TripPA and reference PPA monolayers were characterized by X-ray photoelectron spectroscopy (XPS) and near-edge X-ray absorption fine structure (NEXAFS) spectroscopy and subjected to the work function and contact angle measurements. The experiments were performed at room temperature. The XPS and NEXAFS spectroscopy characterization was conducted at the HE-SGM beamline (bending magnet) of the synchrotron radiation facility BESSY II. A custom-designed multifunctional experimental station, equipped with all necessary tools and detectors, was used.[47] The pressure during the measurements was in the range of $\sim 2 \times 10^{-9}$ Torr.

## 2.4. XPS

The spectra acquisition was carried out in normal emission geometry with a Scienta R3000 electron energy analyzer. The In 3d, C 1s, P 2p, and O 1s spectra, characteristic of both substrate and SAMs, were measured. Primary photon energies (PEs) of 350 eV and 580 eV were used, set in accordance with specific binding energy (BE) range of the spectra. The energy resolution was $\sim$0.3 eV at 350 eV and 0.5 eV at 580 eV. The BE scale of the spectra was referenced to the In $3d_{5/2}$ peak of the ITO substrate at 444.3 eV.[46,48,49] The spectra were fitted, if necessary, by a combination of symmetric Voigt functions and a suitable background.

### 2.5. NEXAFS spectroscopy

The spectra were collected at the carbon and oxygen K-edges with a linearly polarized synchrotron light as the primary source. The polarization factor of the light was ~90%. Partial electron yield detection mode was used. The retarding voltage of the detector was set to −150 V and −350 V for the C and O K-edge, respectively. In the case of the C K-edge, the incidence angle of the primary X-rays with respect to the sample surface was varied in steps between 90° and 20°. The orientation of the electric field vector, ***E***, of the linearly-polarized X-rays was respectively varied between directed parallel to the sample surface and being nearly perpendicular to it. By this means, the dependence of the intensity of the characteristic absorption resonances on the orientation of the respective molecular orbitals with respect to ***E***, termed generally as the linear dichroism effects,[50] was monitored. The analysis of the respective spectra provides information about the orientational order and molecular orientation in the molecular films.[50] In the case of the O K-edge, the spectra were measured at the so-called magic angle of X-ray incidence, 55°, only, providing exclusive information on the electronic structure of the samples, with no admixture of molecular orientation effects.[50]

The PE scale at the C K-edge was referenced to the intense π* resonance of highly oriented pyrolytic graphite at 285.38 eV.[51] The PE scale at the O K-edge was referenced to the two most pronounced resonances in the spectrum of a powder sample of $TiO_2$ (rutile) at 531.3 eV and 534.0 eV.[52] The raw C and O K-edge spectra were divided by the spectra of freshly sputtered ITO and Au samples, respectively, to correct for the PE dependence of the primary X-ray flux. Finally, the spectra were reduced to the standard form[50] by setting the intensity in the pre-edge and post-edge regions to zero and one, respectively.

### 2.6. Work function

Work function measurements were carried out using a UHV Kelvin Probe 2001 system (KP Technology Ltd, UK). The pressure during the measurements was $\sim 10^{-8}$ mbar. The work function values were referenced to that of a hexadecanethiolate (C16) SAM on Au(111), *viz.* 4.32 eV.[53]

### 2.7. Contact angle goniometry

Static contact angles of millipore water were measured with a custom-made, computer-controlled goniometer. The freshly prepared samples were used. The measurements were performed under ambient conditions with the needle tip in contact with the drop. At least three measurements at different locations on each sample were made. The averaged values are reported. Deviations from the average were less than ±2°.

## 3. Results and discussion

### 3.1. XPS

XPS data for the TripPA and PPA films are presented in Fig. 2. The In 3d spectra in Fig. 2a exhibit the In $3d_{5/2,3/2}$ doublet stemming from the substrate. The In $3d_{5/2}$ component was used for the binding energy scale calibration (see Section 2). The intensity of the In 3d signal was utilized to calculate the thickness of the TripPA and PPA films. The signal of the freshly sputtered ITO substrate was used as the reference, the standard, exponential attenuation of this signal by the TripPA/PPA overlayer was assumed,[54] and the attenuation length was set according to the kinetic energy of the In 3d photoelectrons (6.8 Å at 130 eV).[55] The derived thicknesses of the TripPA and PPA films are 11.2 Å and 11.7 Å, respectively, which are quite close to the expected thickness of the respective, PA-anchored monolayers, which is somewhere in the 1.0 nm range.

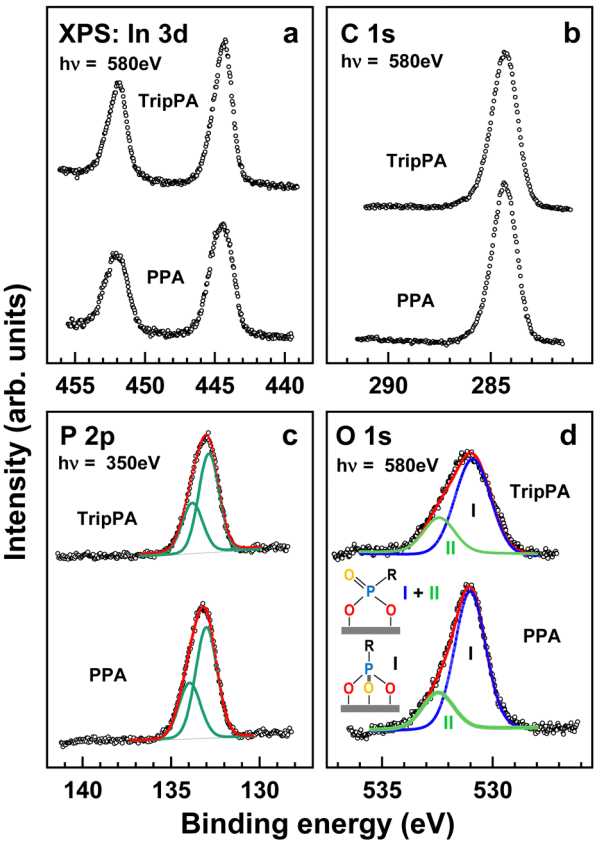


Fig. 2 In 3d (a), C 1s (b), P 2p (c), and O 1s (d) XPS spectra of the TripPA and PPA films on ITO. The P 2p spectra are decomposed in the P $2p_{3/2}$ and P $2p_{3/2}$ components. The O 1s spectra are decomposed in two components, I and II, associated with the specific binding configurations of PA (see text for details). These configurations are schematically shown in (d).

The intensities of the signals are similar for both systems, but the signal of the TripPA film is somewhat higher. The C 1s spectra in Fig. 2b exhibit only one peak at a BE of ~284.3 eV, representative of the triptycene framework in the TripPA case[26] and the benzyl backbone in the PPA case. The intensities of the signals for both samples are quite similar. Significantly, no signal of C=O or COO at a BE of ~288.8 eV, recorded for the blank ITO substrate,[30] is visible, which suggests efficient 'self-cleaning' of the substrate upon the monolayer formation. The CO signal at 285.8 eV, resulting generally in asymmetry of the main peak, is also hardly perceptible, emphasizing the lack of contamination.

The P 2p spectra in Fig. 2c exhibit a single P $2p_{3/2,3/2}$ doublet at BEs of 133.05 eV for the TripPA film and 133.2 eV for the PPA layer. Both these values are distinctly different for that for the unbound PA group (~133.6 eV)[56] and close to that for the PA group anchored to ITO substrate (132.9–133.2 eV)[46,56] The exact bonding configuration of the PA groups, which can generally vary from monodentate to tridentate,[34,57] cannot however be derived from the P 2p XPS spectra, which are hardly sensitive to this parameter.[56]

The bonding configuration of the PA groups in the TripPA and PPA films can however be derived from the substrate-corrected O 1s spectra of these films shown in Fig. 2d (the spectrum of the ITO substrate can be found in ref. 30). According to the recent study of the adsorption of phenylphosphonic acid on $TiO_2$(110), the O 1s spectra of this molecule, close to PPA, exhibits three components at 531.6 (I), 532.7 (II), and 533.8 (III) eV, with the appearance and branching characteristic of the specific configuration mode.[56] A comparably strong and well perceptible 533.8 eV peak is then characteristic of weakly bound PA and monodentate and bidentate onefold deprotonated configurations. In contrast, sole 531.6 eV peak is expected for the tridentate bonding configuration, while in the case of bidentate twofold deprotonated configuration this peak is accompanied by the 532.7 eV shoulder, with the intensity relation of 4 : 1 between these features. Looking at the spectra of the TripPA and PPA films in Fig. 2d, we only find the I and II components at 531.0 and 532.4 eV, respectively, with the distinct dominance of the component I, especially in the PPA case. So, obviously, anchoring of the PA groups in the TripPA and PPA films represents a mixture of the tridentate and bidentate twofold deprotonated configurations. The relative weights of the tridentate configuration in both films could then be estimated at the 65% and 75%, respectively.

Summarizing, according to the XPS data, TripPA film on ITO represents a well-defined and nearly contamination-free tripodal SAM, with the anchoring PA groups in the tridentate and bidentate twofold deprotonated configurations. The effective thickness of this SAM is close to that of the monodentate PPA monolayer, which means similar packing densities in terms of the anchoring groups and about a factor of three difference in the molecular packing density taking into account the numbers of the anchoring groups per TripPA and PPA molecules.

### 3.2. NEXAFS spectroscopy

The C K-edge NEXAFS data for the TripPA and PPA films are presented in Fig. 3. The 'magic angle' (55°) spectra, characteristic of the electronic structure of the films only (see Section 2), are shown in Fig. 3a. The difference between the spectra acquired at the normal (90°) and grazing (20°) incidence, representative of the linear dichroism effects (see Section 2), is depicted in Fig. 3b.

The 55° spectra of both films are similar to each other, with the characteristic shapes typical of the triptycene-based SAMs[26] and methylene-linked monodentate oligophenyl SAMs,[58] respectively. These spectra are dominated by the distict $\pi_1$* resonance (1) accompanied by the less intense $\pi_2$* peak (2) and

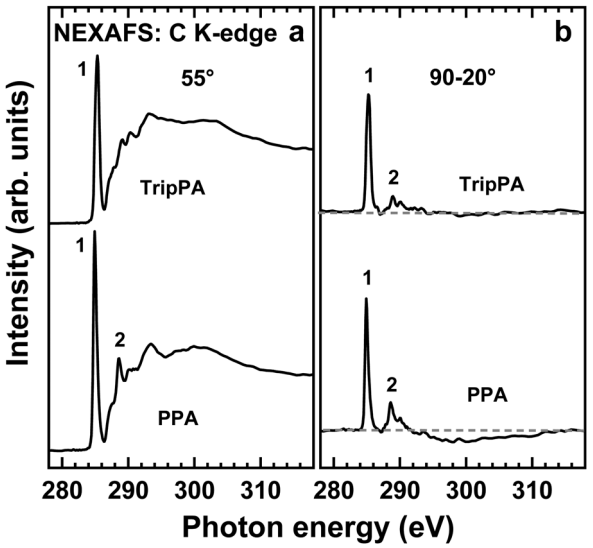


Fig. 3 (a) C K-edge NEXAFS spectra of the TripPA and PPA films acquired at an X-ray incidence angle of 55° and (b) the difference between the spectra acquired at X-ray incidence angles of 90° and 20°. The most important characteristic absorption resonances are marked by numbers (see text for details). The dashed lines in (b) correspond to zero. The vertical scale of panel (b) corresponds to that in panel (a).

a variety of weaker and broader σ*-like features at higher photon energies. The spectra differ distinctly from that of the blank ITO substrate, showing only a weak $\pi_1$*-like signal and dominated by the strong π*(C═O/COOH) resonance.[30] The positions of the $\pi_1$* resonance in the TripPA and PPA spectra, *viz.* 285.3 eV and 285.0 eV, respectively, are characteristic of triptycene and phenyl.[26,50] The relative intensity of the $\pi_1$* and $\pi_2$* resonances with respect to the absorption edge is higher in the PPA case, which is expected and is most likely a consequence of the presence of the interconnecting aliphatic bridge in TripPA. Note that the orbitals associated with the $\pi_1$* and σ* resonances are oriented perpendicular to the planes of the phenyl rings in the SAM-forming molecules and lie within these planes, respectively.

The spectra of both TripPA and PPA films exhibit pronounced linear dichroism (Fig. 3b), which suggests a high orientational order in both systems. Significantly, according to the data in Fig. 3b, the intensity of the π* resonances in the spectra is higher at the normal incidence (90°) comparing to the grazing one (20°), and the σ* resonances exhibit the opposite behavior. Considering the orientation of the respective molecular orbitals with respect to the phenyl rings (see above) and the direction of the electric field vector at the given incidence geometries (see Section 2), an upright orientation of the molecules in both films, with the anchoring groups directed to the substrate (Fig. 1), can be assumed.

Along with the above qualitative conclusions, numerical evaluation of the NEXAFS data was performed relying on the intensity of the most prominent $\pi_1$* resonance, corresponding to the vector-type orbitals directed perpendicular to the planes of the phenyl rings. The schematic geometries of the adsorbed

PPA and TripPA molecules and the relevant parameters are shown and explained in Fig. 4. In the PPA case, the intensity of the $\pi_1$* resonance is described by the equation

$$I = A\{P\cdot 1/3[1 - 1/2(3\cos^2\theta - 1)(3\cos^2\alpha - 1)] + (1 - P)1/2\sin^2\alpha\} \quad (1)$$

where $A$ is a constant, $P$ – polarization factor of the primary X-rays, $\theta$ – angle between $\boldsymbol{E}$ and surface normal, and $\alpha$ – the average tilt angle of the $\pi_1$* orbital with respect to the surface normal.[50,58] The analysis of the NEXAFS data for the PPA film within this equation is performed in Fig. 5a, where we used the intensity ratios instead of the absolute intensity to exclude the unknown constant $A$. The derived value of $\alpha$ is 68 ± 3°. As generally valid for aromatic SAMs, this value is related to the molecular tilt angle $\beta$ by the equation

$$\cos\alpha = \sin\beta \times \cos\gamma \quad (2)$$

where $\gamma$ is the molecular twist angle which is considered to be zero if the $TDM_\pi$ lies in the tilt plane.[58,59] In most cases, this parameter cannot be determined from the NEXAFS data and is, therefore, reasonably assumed or taken from bulk structures, IR data, or simulations. Setting this parameter to the value for bulk biphenyl, *viz.* 32°,[60–62] as frequently done for aromatic SAMs,[58] we got the value of the average tilt angle of 26 ± 3°.

No assumption for $\gamma$ is however necessary in the case of the TripPA film because of the three-fold symmetry of the triptycene framework with respect to the main molecular axis (Fig. 4b). The intensity of the $\pi_1$* resonance as a function of $\theta$ is then described by the equation

$$I = 3BP/2\cdot(3/2\sin^2\beta - 1)\cdot\cos^2\theta + 3B/2\cdot(1 - 1/2\sin^2\beta) \quad (3)$$

where $B$ is a scaling factor and $\beta$ is the average tilt angle of the triptycene units.[63] According to this equation, a plot of the relative intensity of the π* resonance *versus* $\cos^2\theta$ should represent a straight line.[29,63] It was indeed the case for the TripPA film, as shown in Fig. 5b in which the respective plots, for several different intensity ratios, are presented. The fitting of the experimental data by the straight lines according to eqn (3) gives the values of the intercept, $n$, and slope, $m$, of these lines. Using these parameters, the value of $\beta$ was calculated according to the equation[63]

$$\beta = \sin^{-1}\sqrt{\frac{2m + 2Pn}{m + 3Pn}} \quad (4)$$

The derived average tilt angle is 29° ± 3° which is quite close to the analogous value for the PPA film, assuming a similar extent of the orientational order. Obviously, this order is not perfect and the TripPA molecules in the respective monolayer

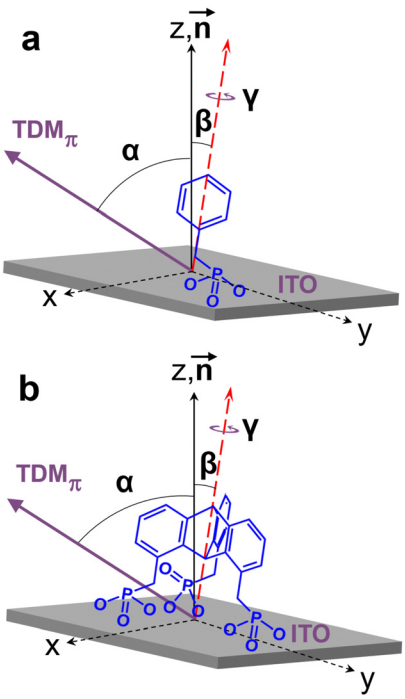


Fig. 4 Schematic of the orientation of PPA (a) and TripPA (b) on the ITO substrate with the relevant parameters: $TDM_\pi$ – transition dipole moment of a π* orbital; $\alpha$ – tilt angle of the $TDM_\pi$; $\beta$ – molecular tilt angle; $\gamma$ – molecular twist angle, **n** – surface normal serving as the reference for $\alpha$ and $\beta$. The molecular axis of PPA is defined with respect to the phenyl ring; that of TripPA is defined with respect to the bridgehead; both axes are drawn by red dashed lines.

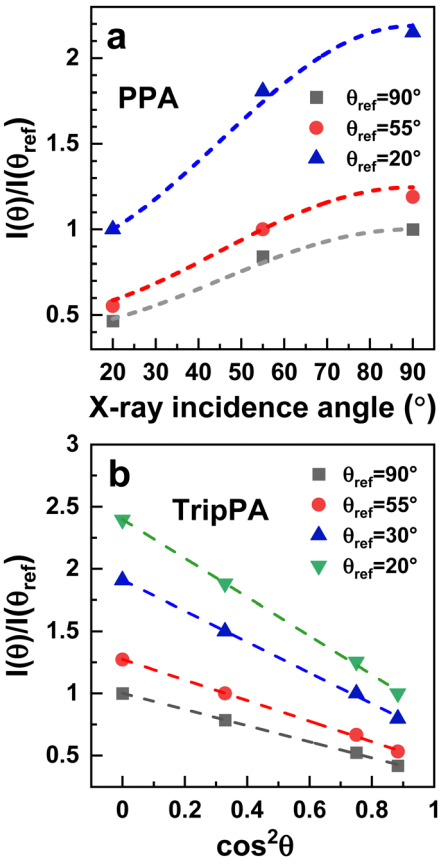


Fig. 5 Evaluation of the average molecular tilt in the PPA (a) and TripPA (b) films according to eqn (1) (a) and eqn (3) (b). The experimental data are shown by symbols, the fitting curves by dashed lines. The legends are given in the panels.

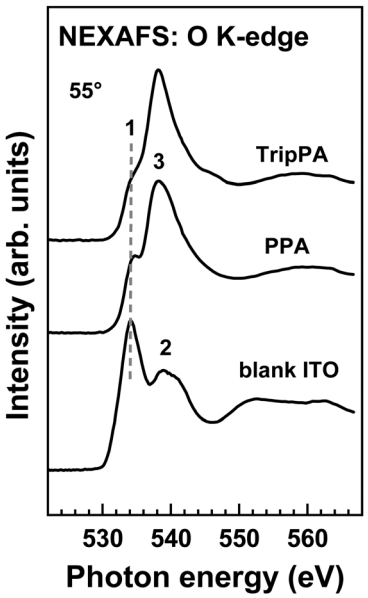


Fig. 6 O K-edge NEXAFS spectra of the TripPA and PPA films and the blank ITO substrate. Characteristic absorption resonances are marked by numbers (see text for details).

are tilted and disordered to some extent, keeping, however, predominant upright orientation, associated with the tripodal bonding configuration (with respect to individual anchoring groups within TripPA).

Complementary information is provided by the O K-edge NEXAFS data, measured for the 'magic angle' (55°) geometry only and presented in Fig. 6. The spectrum of the blank ITO is similar to that of $In_2O_3$,[64] which constitutes ~90% of this mixed oxide. The resonance 1 at 534.1 eV can then be assigned to the oxygen 2p states hybridized to the cation empty 5s states, while the double-resonance feature 2 at 538.5 eV and 540.1 eV is assumed to correspond to the metal 5p states.[64] We think, however, that the quite intense resonance 1 can also contains contributions from the C=O and COOH groups at the surface of the ITO substrate, since the most pronounced π* resonance of these groups lies in the same excitation energy range.[65,66]

The spectra of the TripPA and PPA films are similar to each other but differ drastically from that of the blank ITO. The resonance 1 is significantly reduced in intensity and the dominant feature is a resonance 3 at ~538.2 eV. This dominance and the entire shape of the spectra is close to that of phosphonic acid,[67] suggesting that these spectra are mostly representative of the TripPA and PPA films and the signal of the substrate is strongly attenuated by these overlayers. It is however difficult to make any conclusion about the bonding configuration of the PA anchoring groups on the basis of the O K-edge NEXAFS spectra (as it was done in the case of O 1s XPS) because of the lack of necessary reference data.

Summarizing, the NEXAFS data support the statement regarding the formation of well-defined and nearly contamination-free TripPA SAM on ITO. The orientational order in this SAM is close to that in the reference, monopodal PPA monolayer. The average molecular inclination in both films was evaluated.

### 3.3. Work function

Work function (WF) is an important parameter in the context of energy level alignment in organic electronics and photovoltaics. It is also an important fingerprint parameter to monitor the effect of monomolecular films on the electrostatic properties of surfaces and interfaces.

For ITO, a variety of different WF values, varied from 4.0 to 5.2 eV, was reported,[46,68,69] related most likely to the different preparation conditions. For our substrates, we measured ~4.7 eV for the blank ITO and ~4.2 eV for the freshly sputtered ITO. In view of the self-cleaning process occurred during the SAM assembly, we rather favor the latter value as the reference for the SAM values but cannot exclude that the real value could be somewhat higher. Assembly of PPA and TripPA led to the WF increase with respect to the reference value, with the larger effect of TripPA (+0.48 eV *vs.* +0.25 eV). The difference can be related to the variation in the extent of the self-cleaning and the difference in the bonding configuration (see Section 3.1).

Decoration of the TripPA with the polar cyano group (2.98 D for HCN),[70] shown in Fig. 7 (NC-TripPA), results in the WF increase by *ca.* +0.3 eV. This value can be compared with the impact of this group on the work function of the densely packed SAMs of phenylthiol and thiol-decorated triptycene on Au(111).[29] Such a decoration, with the density of cyano groups of $4.45 \times 10^{14}$ $cm^{-1}$ in the latter film, resulted in the WF increase by *ca.* +0.65 eV compared to the non-substituted case.[29] Considering that the triptycene molecules in ref. 29 were decorated at the *para*-positions of the rings (three groups pro molecule) in contrast to the bridgehead position in the present case (one group pro molecule), three times lesser effect (+0.22 eV) can be expected at the same packing density and

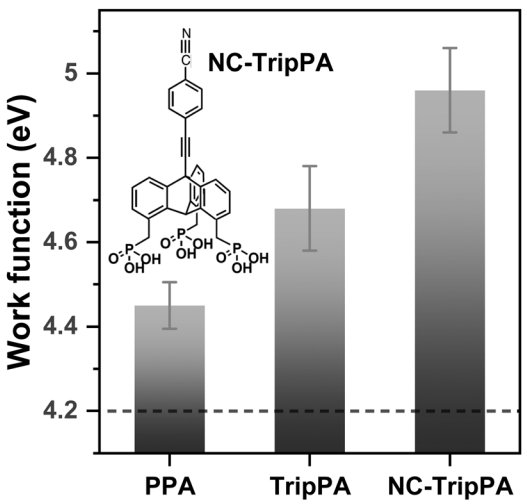


Fig. 7 Work function of the PPA, TripPA, and NC-Trip-PA SAMs on ITO. The horizonal dashed line represents the work function of the sputtered ITO substrate. Molecular structure of NC-TripPA is shown. The quality of the NC-TripPA monolayer was verified by complementary spectroscopic experiments (the data are not shown).

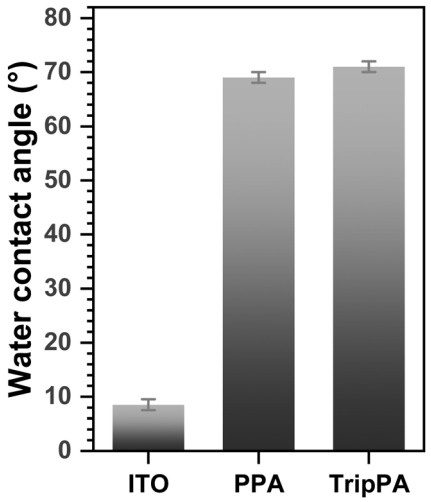


Fig. 8 Static WCAs of the blank and PPA and TripPA covered ITO substrate.

molecular orientation. Obviously, the observed effect for the NC-TripPA film is even larger, which is an evidence for the dense molecular packing and better alignment of the tail groups and, consequently, for potential of TripPA-based SAMs for electrostatic engineering of surfaces and interfaces. An even stronger WF effect (by a factor of 3) can then be achieved at the decoration of the *para*-positions of the Trip-PA rings, using the –CN groups (similar to ref. 29) or other polar moieties.

### 3.4. Wetting properties

Along with the work function, wetting properties of the SAM-modified interface are of importance both in the context of applications (*e.g.*, corrosion protection) and as a fingerprint of the SAM formation. In the present case, these properties were monitored by the contact angle goniometry. The static water contact angles (WCA) of the as-received ITO substrates was 74 ± 1° which, however, was reduced to 8.5 ± 1° after the cleaning and UV treatment (blank ITO; see Section 2 for details). The latter value, considered as the reference for the SAM values, is presumably related to the intrinsic high hydrophilicity of the ITO surface.[71] The formation of the Trip-PA and PPA films resulted in the significant WCA increase, as shown in Fig. 8 where the respective values are presented. The WCAs of these films, 71 ± 1° and 69 ± 1°, respectively, are very close to each other and close as well to the average value of the advancing and receding WCAs for the SAM of non-substituted biphenylthiols on gold (71°),[72] serving as a reasonable reference for densely packed and well-defined aromatic monolayers. Consequently, high packing density and good quality can be assumed for the Trip-PA and PPA films as well, in good agreement with the spectroscopic and WF data (Sections 3.1–3.3).

### 3.5. Comparison with TripCA

As mentioned in Section 1, triptycene SAMs with the carboxylic acid anchoring groups, directly attached to the *para* positions of the phenyl rings (1,8,13-tricarboxy-triptycene; TripCA), were assembled recently on the ITO substrates, prepared in the same fashion as the substrates in the present study.[30] So, a direct comparison of the TripPA SAM and the best-quality TripCA monolayer (the parameters of the preparation procedure were varied)[30] can be performed. This comparison is presented in Table 1. Accordingly, the major parameters of the TripPA and TripCA SAM are similar, suggesting comparable quality and packing densities. The slightly higher effective thickness of the TripPA SAM is presumably related to the presence of the methylene linker in the anchoring groups (Fig. 1). The molecular orientation and orientational order in the TripPA SAM are however superior to those in the TripCA monolayer, as evidenced by the smaller value of the average molecular tilt angle. Note also that phosphonic acids provide generally more robust bonds to oxides compared to their carboxylic acid counterparts,[34] which can be of advantage for the thermal and chemical stability of the former films.

Table 1 Comparison between the parameters of the TripPA (this work) and TripCA[30] SAMs. The accuracies of these parameters are ±0.5 Å, ±3°, ±0.05 V, and ±1–2°, respectively

| SAM | Effective thickness (Å) | Average tilt angle (°) | Work function (eV) | Static water contact angle (°) |
|---|---|---|---|---|
| TripPA | 11.2 | 29 | 4.68 | 71 |
| TripCA | 10 | 32.5 | 4.78 | 69 |

## 4. Conclusions

Using a combination of several complementary experimental techniques, we studied self-assembly of TripPA on ITO, considered as a representative and application-relevant oxide substrate. As the reference to this tripodal system, we took PPA as the closest monopodal system, corresponding to an individual 'blade' of TripPA. All experimental data consistently suggest formation of well-defined, densely packed, and nearly contamination-free tripodal TripPA SAMs on ITO. The anchoring to the substrate in this SAM corresponds to a mixture of the tridentate and bidentate twofold deprotonated configurations, with the preference of the former bonding mode. The packing density (in terms of the PA groups) and orientational order in the TripPA SAM were found to be close to those in the reference PPA monolayer. It was also demonstrated that the assembly of the TripPA SAM results in the similar effect as the PPA monolayer in the context of modification of the wetting properties and the work function of the substrate. Additional experiments with NC-TripPA confirm the high packing density of the TripPA SAM and show the effect of polar tail groups on the work function.

Summarizing, the results of the present study demonstrate a good potential of TripPA as a robust and versatile tripodal platform for oxide substrate engineering, including tuning of the work function. This basic molecule can be flexibly decorated with suitable functional tail groups meeting requirements of specific applications.

 

## Conflicts of interest

There are no conflicts to declare.

## Acknowledgements

We thank the Helmholtz Zentrum Berlin (HZB) for the allocation of synchrotron radiation beamtime at BESSY II and financial support. We thank Dr M. Brzhezinskaya (HZB) for the assistance during the experiments at the synchrotron. The work was financially supported by the German Research Foundation (Deutsche Forschungsgemeinschaft; DFG) *via* grant ZH 63/39-1 (C. Z., S. D. and M. Z.) and CREST (Japan Science and Technology Agency; JST) *via* grant JPMJCR18I4 (T. F.) and also supported in part by ''Dynamic Alliance for Open Innovation Bridging Human, Environment and Materials'' from MEXT, Japan.

## References

1 J. C. Love, L. A. Estroff, J. K. Kriebel, R. G. Nuzzo and G. M. Whitesides, Self-assembled monolayers of thiolates on metals as a form of nanotechnology, *Chem. Rev.*, 2005, **105**, 1103–1170.
2 M. Kind and C. Wöll, Organic surfaces exposed by self-assembled organothiol monolayers: Preparation, characterization, and application, *Prog. Surf. Sci.*, 2009, **84**, 230–278.
3 S. Flink, F. C. J. M. van Veggel and D. N. Reinhoudt, Sensor functionalities in self-assembled monolayers, *Adv. Mater.*, 2000, **12**, 1315–1328.
4 D. Samanta and A. Sarkar, Immobilization of bio-macromolecules on self-assembled monolayers: Methods and sensor applications, *Chem. Soc. Rev.*, 2011, **40**, 2567–2592.
5 A. Turchanin and A. Golzhauser, Carbon nanomembranes, *Adv. Mater.*, 2016, **28**, 6075–6103.
6 A. Terfort and M. Zharnikov, Electron-irradiation promoted exchange reaction as a tool for surface engineering and chemical lithography, *Adv. Mat. Interfaces*, 2021, **8**, 2100148.
7 M. Halik and A. Hirsch, The Potential of Molecular Self-assembled monolayers in organic electronic devices, *Adv. Mater.*, 2011, **23**, 2689–2695.
8 A. Vilan, D. Aswal and D. Cahen, Large-area, ensemble molecular electronics: Motivation and challenges, *Chem. Rev.*, 2017, **117**, 4248–4286.
9 A. S. Sizov, E. V. Agina and S. A. Ponomarenko, Self-assembled interface monolayers for organic and hybrid electronics, *Russ. Chem. Rev.*, 2019, **88**, 1220–1247.
10 G. D. Kong, S. E. Byeon, S. Park, H. Song, S.-Y. Kim and H. J. Yoon, Mixed Molecular Electronics: Tunneling behaviors and applications of mixed self-assembled monolayers, *Adv. Electron. Mater.*, 2020, **6**, 1901157.
11 R. Gupta, J. A. Fereiro, A. Bayat, A. Pritam, M. Zharnikov and P. C. Mondal, Nanoscale molecular rectifiers, *Nat. Rev. Chem.*, 2023, **7**, 106–122.
12 P. Chinwangso, A. C. Jamison and T. R. Lee, Multidentate adsorbates for self-assembled monolayer films, *Acc. Chem. Res.*, 2011, **44**, 511–519.
13 M. Valášek, M. Lindner and M. Mayor, Rigid multipodal platforms for metal surfaces, *Beilstein J. Nanotechnol.*, 2016, **7**, 374–405.
14 Z.-Q. Li, J.-H. Tang and Y.-W. Zhong, Multidentate anchors for surface functionalization, *Chem. – Asian J.*, 2019, **14**, 3119–3126.
15 D. Hirayama, K. Takimiya, Y. Aso, T. Otsubo, T. Hasobe, H. Yamada, H. Imahori, S. Fukuzumi and Y. Sakata, Large photocurrent generation of gold electrodes modified with [60]fullerene-linked oligothiophenes bearing a tripodal rigid anchor, *J. Am. Chem. Soc.*, 2002, **124**, 532–533.
16 T. Weidner, A. Krämer, C. Bruhn, M. Zharnikov, A. Shaporenko, U. Siemeling and F. Träger, Novel tripod ligands for prickly self-assembled monolayers, *Dalton Trans.*, 2006, 2767–2777.
17 K. Nikitin, E. Lestini, M. Lazzari, S. Altobello and D. Fitzmaurice, A Tripodal [2]rotaxane on the surface of gold, *Langmuir*, 2007, **23**, 12147–12153.
18 T. Weidner, N. Ballav, U. Siemeling, D. Troegel, T. Walter, R. Tacke, D. G. Castner and M. Zharnikov, Tripodal binding units for self-assembled monolayers on gold: A comparison of thiol and thioether headgroups, *J. Phys. Chem. C*, 2009, **113**, 19609–19617.
19 S. Ramachandra, K. C. Schuermann, F. Edafe, P. Belser, C. A. Nijhuis, W. F. Reus, G. M. Whitesides and L. De Cola, Luminescent ruthenium tripod complexes: Properties in solution and on conductive surfaces, *Inorg. Chem.*, 2011, **50**, 1581–1591.
20 S.-E. Zhu, Y.-M. Kuang, F. Geng, J.-Z. Zhu, C.-Z. Wang, Y.-J. Yu, Y. Luo, Y. Xiao, K.-Q. Liu, Q.-S. Meng, L. Zhang, S. Jiang, Y. Zhang, G.-W. Wang, Z.-C. Dong and J. G. Hou, Self-decoupled porphyrin with a tripodal anchor for molecular-scale electroluminescence, *J. Am. Chem. Soc.*, 2013, **135**, 15794–15800.
21 T. Kitagawa, H. Matsubara, K. Komatsu, K. Hirai, T. Okazaki and T. Hase, Ideal redox behavior of the high-density self-assembled monolayer of a molecular tripod on a Au111 surface with a terminal ferrocene group, *Langmuir*, 2013, **29**, 4275–4282.
22 R. Sakamato, Y. Ohirabaru, R. Matsuoka, H. Maeda, S. Katagiri and H. Nishihara, Orthogonal bis(terpyridine)–Fe(II) metal complex oligomer wires on a tripodal scaffold: Rapid electron transport, *Chem. Commun.*, 2013, **49**, 7108–7110.
23 K.-Y. Chen, O. Ivashenko, G. T. Carroll, J. Robertus, J. C. M. Kistemaker, G. London, W. R. Browne, P. Rudolf and B. L. Feringa, Control of surface wettability using tripodal light-activated molecular motors, *J. Am. Chem. Soc.*, 2014, **136**, 3219–3224.
24 M. Lindner, M. Valášek, J. Homberg, K. Edelmann, L. Gerhard, W. Wulfhekel, O. Fuhr, T. Wächter, M. Zharnikov, V. Kolivoška, L. Pospísil, G. Meszaros, M. Hromadova and M. Mayor, Importance of the anchor group position (para

*versus* meta) in tetraphenylmethane tripods: Synthesis and self-assembly features, *Chem. – Eur. J.*, 2016, **22**, 13218–13235.

25 M. Sánchez-Molina, A. Díaz, E. Sauter, M. Zharnikov and J. M. López-Romero, Tripod-shaped molecules: Synthesis and immobilization on Au(111) substrates, *Appl. Surf. Sci.*, 2019, **470**, 259–268.

26 F. Ishiwari, G. Nascimbeni, E. Sauter, H. Tago, Y. Shoji, S. Fujii, M. Kiguchi, T. Tada, M. Zharnikov, E. Zojer and T. Fukushima, Triptycene tripods for the formation of highly uniform and densely packed self-assembled monolayers with controlled molecular orientation, *J. Am. Chem. Soc.*, 2019, **141**, 5995–6005.

27 T. Tada, F. Ishiwari, Y. Shoji and T. Fukushima, First-principles study of the adsorption behavior of triptycene molecular tripods on Au(111): Site-selectivity and unambiguous molecular orientation, *J. Phys. Chem. C*, 2019, **123**, 4401–4406.

28 S. Das, G. Nascimbeni, R. O. de la Morena, F. Ishiwari, Y. Shoji, T. Fukushima, M. Buck, E. Zojer and M. Zharnikov, Porous honeycomb self-assembled monolayers: Tripodal adsorption and hidden chirality of carboxylate anchored triptycenes on Ag, *ACS Nano*, 2021, **15**, 11168–11179.

29 S. Das, A. Asyuda, Y. Shoji, A. Kosaka, T. Fukushima and M. Zharnikov, Cyano-substituted triptycene-based monolayers on Au(111): Tripodal adsorption, dipole engineering, and charge transfer, *J. Phys. Chem. C*, 2021, **125**, 18968–18978.

30 S. Das, F. Ishiwari, Y. Shoji, T. Fukushima and M. Zharnikov, Triptycene-based tripodal self-assembled monolayer on indium tin oxide, *J. Phys. Chem. C*, 2023, **127**, 2088–2097.

31 S. Das, F. Ishiwari, Y. Shoji, T. Fukushima and M. Zharnikov, Triptycene-based self-assembled monolayer as a template for successive click reactions, *J. Phys. Chem. C*, 2023, **127**, 5178–5185.

32 Z. Zhao, T. Fukushima and M. Zharnikov, Electron-induced modification of triptycene self-assembled monolayer in context of lithography and nanofabrication, *J. Phys. Chem. C*, 2023, **127**, 15582–15590.

33 Y. Liu, S. Sanjayan, Y. Shoji, T. Fukushima and M. Zharnikov, Appearance of different conductance states in monomolecular films of ferrocene-decorated triptycene-based tripods, *J. Phys. Chem. C*, 2023, **127**, 24458–24466.

34 S. A. Paniagua, A. J. Giordano, O. N. L. Smith, S. Barlow, H. Li, N. R. Armstrong, J. E. Pemberton, J.-L. Bredas, D. Ginger and S. R. Marder, Phosphonic acids for interfacial engineering of transparent conductive oxides, *Chem. Rev.*, 2016, **116**, 7117–7158.

35 J. E. McDermott, M. McDowell, I. G. Hill, J. Hwang, A. Kahn, S. L. Bernasek and J. Schwartz, Organophosphonate self-assembled monolayers for gate dielectric surface modification of pentacene-based organic thin-film transistors: A comparative study, *J. Phys. Chem. A*, 2007, **111**, 12333–12338.

36 S. Lacher, Y. Matsuo and E. Nakamura, Molecular and supramolecular control of the work function of an inorganic electrode with self-assembled monolayer of umbrella-shaped fullerene derivatives, *J. Am. Chem. Soc.*, 2011, **133**, 16997–17004.

37 U. Koldemir, J. L. Braid, A. Morgenstern, M. Eberhart, R. T. Collins, D. C. Olson and A. Sellinger, Molecular design for tuning work functions of transparent conducting electrodes, *J. Phys. Chem. Lett.*, 2015, **6**, 2269–2276.

38 M. Timpel, H. Li, M. V. Nardi, B. Wegner, J. Frisch, P. J. Hotchkiss, S. R. Marder, S. Barlow, J.-L. Brédas and N. Koch, Electrode work function engineering with phosphonic acid monolayers and molecular acceptors: Charge redistribution mechanisms, *Adv. Funct. Mater.*, 2018, **28**, 1704438.

39 Y. Lin, Y. Firdaus, F. H. Isikgor, M. I. Nugraha, E. Yengel, G. T. Harrison, R. Hallani, A. El-Labban, H. Faber, C. Ma, X. Zheng, A. Subbiah, C. T. Howells, O. M. Bakr, I. McCulloch, S. D. Wolf, L. Tsetseris and T. D. Anthopoulos, Self-assembled monolayer enables hole transport layer-free organic solar cells with 18% efficiency and improved operational stability, *ACS Energy Lett.*, 2020, **5**, 2935–2944.

40 H. Chen, W. Zhang, M. Li, G. He and X. Guo, Interface engineering in organic field-effect transistors: Principles, applications, and perspectives, *Chem. Rev.*, 2020, **120**, 2879–2949.

41 D. Song, S. Narra, M.-Y. Li, J.-S. Lin and E. W.-G. Diau, Interfacial engineering with a hole-selective self-assembled monolayer for tin perovskite solar cells via a two-step fabrication, *ACS Energy Lett.*, 2021, **6**, 4179–4186.

42 Z.-R. Lan, J.-Y. Shao and Y.-W. Zhong, Self-assembled monolayers as hole-transporting materials for inverted perovskite solar cells, *Mol. Syst. Des. Eng.*, 2023, **8**, 1440–1455.

43 C. Donley, D. Dunphy, D. Paine, C. Carter, K. Nebesny, P. Lee, D. Alloway and N. R. Armstrong, Characterization of indium−tin oxide interfaces using X-ray photoelectron spectroscopy and redox processes of a chemisorbed probe molecule: Effect of surface pretreatment conditions, *Langmuir*, 2002, **18**, 450–457.

44 Y. J. Jeong, S. Woo, Y. Kim, S. J. Jeong, Y. S. Han, D. K. Lee, J. I. I. Ko, S.-K. Jung and B. C. An, Effects of solvents on ITO cracks in ultrasonic cleaning of ITO-coated flexible substrates for polymer solar cells, *Mol. Cryst. Liq.*, 2011, **551**, 212–220.

45 X. Chen, E. Luais, N. Darwish, S. Ciampi, P. Thordarson and J. J. Gooding, Studies on the effect of solvents on self-assembled monolayers formed from organophosphonic acids on indium tin oxide, *Langmuir*, 2012, **28**, 9487–9495.

46 A. Asyuda, M. Gärtner, X. Wan, I. Burkhart, T. Saßmannshausen, A. Terfort and M. Zharnikov, Self-assembled monolayers with embedded dipole moments for work function engineering of oxide substrates, *J. Phys. Chem. C*, 2020, **124**, 8775–8785.

47 A. Nefedov and C. Wöll, *Advanced applications of NEXAFS spectroscopy for functionalized surfaces*, ed. G. Bracco and B. Holst, Springer-Verlag, Berlin, 2013, vol. 51, pp. 277–303.

48 J. F. Moulder, W. E. Stickle, P. E. Sobol and K. D. Bomben, *Handbook of X-ray photoelectron spectroscopy*, ed. J. Chastian, PerkinElmer Corp., Eden Prairie, MN, 1992.

49 V. Georgieva, M. Aleksandrova, P. Stefanov, A. Grechnikov, V. Gadjanova, T. Dilova and T. Angelov, Study of quartz

crystal microbalance $NO_2$ sensor coated with sputtered indium tin oxide film, *J. Phys.: Conf. Ser.*, 2014, **558**, 012037.
50 J. Stöhr, *NEXAFS Spectroscopy*, Springer-Verlag, Berlin, 1992.
51 P. E. Batson, Carbon 1s near-edge-absorption fine structure in graphite, *Phys. Rev. B*, 1993, **48**, 2608–2610.
52 V. S. Lusvardi, M. A. Barteau, J. G. Chen, J. Eng, Jr., B. Frühberger and A. Teplyakov, An NEXAFS investigation of the reduction and reoxidation of $TiO_2$(001), *Surf. Sci.*, 1998, **397**, 237–250.
53 O. M. Cabarcos, S. Schuster, I. Hehn, P. P. Zhang, M. M. Maitani, N. Sullivan, J. B. Giguère, J. F. Morin, P. S. Weiss, E. Zojer, M. Zharnikov and D. L. Allara, Effects of embedded dipole layers on electrostatic properties of alkanethiolate self-assembled monolayers, *J. Phys. Chem. C*, 2017, **121**, 15815–15830.
54 M. Ratner and D. Castner, Electron spectroscopy for chemical analysis, in *Surface analysis - The principal techniques*, ed. J. Vickerman, Wiley, Chichester, 1997.
55 C. L. A. Lamont and J. Wilkes, Attenuation length of electrons in self-assembled monolayers of *n*-alkanethiols on gold, *Langmuir*, 1999, **15**, 2037–2042.
56 J. Köbl, D. Wechsler, E. Y. Kataev, F. J. Williams, N. Tsud, S. Franchi, H.-P. Steinrück and O. Lytken, Adsorption of phenylphosphonic acid on rutile $TiO_2$(110), *Surf. Sci.*, 2020, **698**, 121612.
57 S. P. Pujari, L. Scheres, A. T. M. Marcelis and H. Zuilhof, Covalent surface modification of oxide surfaces, *Angew. Chem., Int. Ed.*, 2014, **53**, 6322–6356.
58 M. Zharnikov, Near-edge X-ray absorption fine structure spectroscopy in studies of self-assembled monomolecular films, *J. Electron Spectrosc. Relat. Phenom.*, 2023, **264**, 147322.
59 H.-T. Rong, S. Frey, Y.-J. Yang, M. Zharnikov, M. Buck, M. Wühn, Ch Wöll and G. Helmchen, On the importance of the head group substrate bond in thiol monolayers: A study of biphenyl based thiols on gold and silver, *Langmuir*, 2001, **17**, 1582–1593.
60 J. Trotter, The crystal and molecular structure of biphenyl, *Acta Crystallogr.*, 1961, **14**, 1135–1140.
61 A. Hargreaves and S. H. Rizvi, The crystal and molecular structure of biphenyl, *Acta Crystallogr.*, 1962, **15**, 365–373.
62 G.-P. Charbonneau and Y. Delugeard, Structural transition in polyphenyls. III. Crystal structure of biphenyl at 110 K, *Acta Crystallogr., Sect. B: Struct. Crystallogr. Cryst. Chem.*, 1976, **26**, 1420–1423.
63 J. Liu, M. Kind, B. Schüpbach, D. Käfer, S. Winkler, W. Zhang, A. Terfort and C. Wöll, Triptycene-terminated thiolate and selenolate monolayers on Au(111), *Beilstein J. Nanotechnol.*, 2017, **8**, 892–905.
64 T. De Boer, M. Bekheet, A. Gurlo, R. Riedel and A. Moewes, Band gap and electronic structure of cubic, rhombohedral, and orthorhombic $In_2O_3$ polymorphs: Experiment and theory, *Phys. Rev. B: Condens. Matter Mater. Phys.*, 2016, **93**, 155205.
65 S. G. Urquhart and H. Ade, Trends in the carbonyl core (C 1S, O 1S) → $\pi^*_{C=O}$ transition in the near-edge X-ray absorption fine structure spectra of organic molecules, *J. Phys. Chem. B*, 2002, **106**, 8531–8538.
66 F. Frati, M. O. J. Y. Hunault and F. M. F. de Groot, Oxygen K-edge X-ray absorption spectra, *Chem. Rev.*, 2020, **120**, 4056–4110.
67 N. T. Samuel, C.-Y. Lee, L. J. Gamble, D. A. Fischer and D. G. Castner, NEXAFS characterization of DNA components and molecularorientation of surface-bound DNA oligomers, *J. Electron Spectrosc. Relat. Phenom.*, 2006, **152**, 134–142.
68 H. Li, P. Winget and J.-L. Brédas, Transparent conducting oxides of relevance to organic electronics: Electronic structures of their interfaces with organic layers, *Chem. Mater.*, 2014, **26**, 631–646.
69 J. Rittich, S. Jung, J. Siekmann and M. Wuttig, Indium-Tin-Oxide (ITO) Work Function tailoring by covalently bound carboxylic acid self-assembled monolayers, *Phys. Status Solidi B*, 2018, **255**, 1800075.
70 R. D. Nelson, Jr., D. R. Lide and A. A. Maryott, *Selected values of electric dipole moments for molecules in the gas phase*, National Standard Reference Data Series - National Bureau of Standards 10, National Bureau of Standards, 1967.
71 H. Di, W. Jiang, H. Sun, C. Zhao, F. Liao and Y. Zhao, Effects of ITO substrate hydrophobicity on crystallization and properties of $MAPbBr_3$ single-crystal thin films, *ACS Omega*, 2020, **5**, 23111–23117.
72 J. F. Kang, A. Ulman, S. Liao, R. Jordan, G. H. Yang and G. Y. Liu, Self-assembled rigid monolayers of 4′-substituted-4-mercaptobiphenyls on gold and silver surfaces, *Langmuir*, 2001, **17**, 95–106.